Supporting Information for

A homochiral Zn-Dy heterometallic left-handed helical chain complex without chiral ligands: anion-induced assembly and multifunctional integration

Cai-Ming Liu,[a,*] De-Qing Zhang,[a,*] Ren-Gen Xiong,[b,*] Xiang Hao,[a] and Dao-Ben Zhu[a]

[a] *Beijing National Laboratory for Molecular Sciences, Center for Molecular Science, Key Laboratory of Organic Solids, Institute of Chemistry, CAS Research/Education Center for Excellence in Molecular Science, Chinese Academy of Sciences, Beijing 100190, China*

[b] *Ordered Matter Science Research Center, Southeast University, Nanjing 211189, China*

Experimental Section

All starting materials are commercially available and analytically pure. The elemental analyses were carried out on a Heraeus Chn-Rapid elemental analyzer. The infrared spectra were measured on a Pekin-Elmer 2000 spectrophotometer with pressed KBr pellets. The X-ray powder diffraction (XRD) pattern was recorded on a Rigaku D/max 2500 diffractometer with Cu-Kα (λ = 1.5418 Å) radiation. The solid state vibrational circular dichroism (VCD) spectrum was recorded on a Bruker PMA 50 spectrometer. The magnetic susceptibility measurements were carried out on polycrystalline samples with a Quantum Design MPMS-XL5 SQUID magnetometer in the temperature range 1.9-300 K. Diamagnetic corrections were estimated from Pascal's constants for all constituent atoms.

Caution! *Perchlorate salts or perchlorate complexes are potentially explosive and should be handled with care and used only in small amounts.*

Preparation of 1. Zn(L)(H_2O) (0.2 mmol), $Dy(ClO_4)_3 \cdot 6H_2O$ (0.1 mmol) and 2,2′-bipyridine-6,6′-dicarboxylic acid (0.1 mmol) and 10 mL methanol were stirred at room temperature for 10 min, this mixture was then transferred into 25 mL Teflon-lined stainless steel vessel and maintained at 100 °C for 5 days under autogenous pressure. After the autoclave had cooled to room temperature at rate of 0.15 ºC/min, yellow plate crystals of **1** were harvested, washed with methanol and then dried at ambient temperature. Yield: 35% based on Dy. Elemental analysis (%): calc. for $C_{64}H_{60}ClDyN_8O_{22}Zn_3$ (**1**): C, 45.55; H, 3.58; N, 6.64. Found: C, 45.60; H, 3.62; N, 6.56. IR(KBr, cm^{-1}): 3440(br, m), 3083(w), 2934(w), 2853(w), 1626(vs), 1596(s), 1575(m), 1473(m), 1437(w), 1409 (m), 1385(w), 1360(w), 1315(w), 1294(w), 1249(w), 1223(m), 1194(w), 1172(w), 1121(m), 1093(m), 1019(w), 977(w), 954(w), 921(w), 913(w), 850(w), 783(m), 744(w), 722(w), 705(w), 677(w), 635(w), 625(w).

Alternative Method: The procedure is the same as above but using $Dy(CH_3CO_2)_3 \cdot 4H_2O$ (0.1 mmol) and $Zn(ClO_4)_3 \cdot 6H_2O$ (0.1 mmol) instead of $Dy(ClO_4)_3 \cdot 6H_2O$ (0.1 mmol). Yield: 45% based on Dy.

Preparation of 2: The procedure was the same as that for **1** but using $Dy(CH_3CO_2)_3{\cdot}4H_2O$ (0.1 mmol) or $Dy_2(SO_3)_3{\cdot}8H_2O$ (0.05 mmol) instead of $Dy(ClO_4)_3{\cdot}6H_2O$ (0.1 mmol). Yellowish needle crystals of **2** were obtained, washed with methanol and then dried at ambient temperature.Yield: 15-20% based on Dy. Elemental analysis (%): calc. for $C_{88}H_{79}Dy_2N_{12}O_{29.5}Zn_3$ (**2**): C, 46.00; H, 3.47; N, 7.31. Found: C, 45.92; H, 3.53; N, 7.25. IR (KBr, cm^{-1}): 3420(br, s), 3085(w), 2933(w), 2857(w), 2838(w), 1626(s), 1597(s), 1573(m), 1475(w), 1463(m), 1410(m), 1369(s), 1315(w), 1291(w), 1275(w), 1249(w), 1223(m), 1192(w), 1160(w), 1087(w), 1076(w), 1020(w), 978(w), 954(w), 913(w), 852(w), 777(m), 741(w), 721(w), 677(w), 643(w), 641(w), 477(w), 429(w).

X-ray crystallography: Data were collected at 173(2) K on a Rigaku ST-Saturn724+ CCD diffractometer with *Mo-Kα* radiation (λ = 0.71073 Å). Cell parameters were obtained by the global refinement of the positions of all collected reflections for two complexes. The structure was solved by direct methods and refined by a full matrix least-squares technique based on F^2 using SHELXL-2018 program. All non-hydrogen atoms were refined anisotropically, and all hydrogen atoms were refined as riding atoms. Notably, the lattice guest molecules in **2** were disordered, which reduce the quality of crystal structures obviously, so the SQUEEZE routine in PLATON was applied to give better refinement.

Second harmonic generation (SHG) experiments: An unexpanded laser beam with low divergence (pulsed Nd:YAG at a wavelength of 1064 nm, 5 ns pulse duration, 1.6 MW peak power, 10 Hz repetition rate) was used. The instrument model is Ins 1210058, INSTEC Instruments, while the laser is Vibrant 355 II, OPOTEK. The numerical values of the nonlinear optical coefficients for SHG have been determined by comparison with a KDP reference.

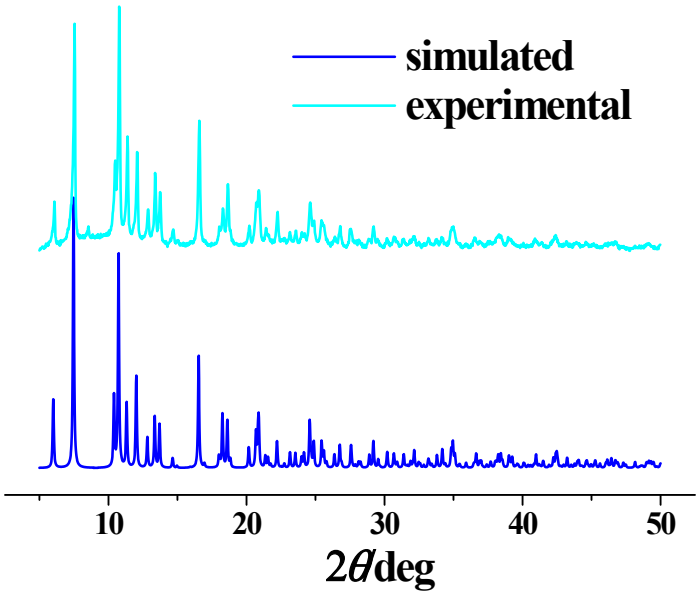

Fig. S1. The simulative and experimental powder X-ray diffraction patterns for **1**.

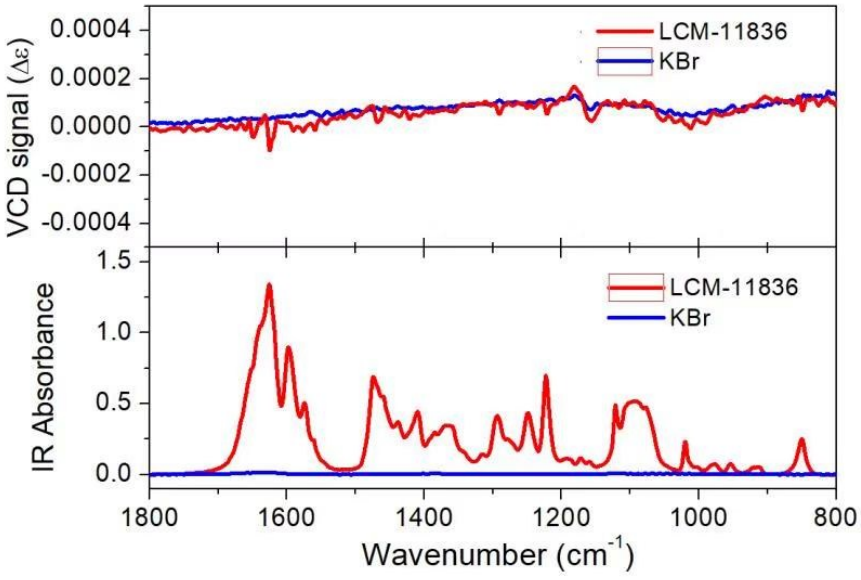

Fig. S2. The solid-state VCD and IR spectra of **1** in a KBr matrix including 1% (wt) crystal grains at room temperature.

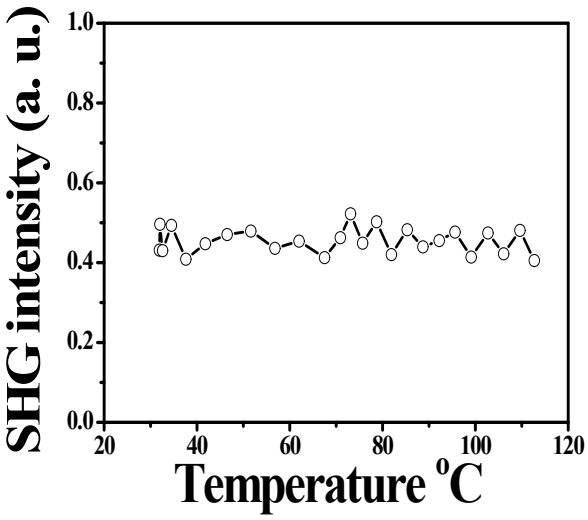

Fig. S3. Temperature dependence of second-order nonlinear optical coefficient of **1** (heating).

Table S1. Continuous Shape Measures calculation for Dy1 atom in **1**.

Dy1 structure

OP-8	1 D8h	Octagon
HPY-8	2 C7v	Heptagonal pyramid
HBPY-8	3 D6h	Hexagonal bipyramid
CU-8	4 Oh	Cube
SAPR-8	5 D4d	Square antiprism
TDD-8	6 D2d	Triangular dodecahedron
JGBF-8	7 D2d	Johnson gyrobifastigium J26
JETBPY-8	8 D3h	Johnson elongated triangular bipyramid J14
JBTPR-8	9 C2v	Biaugmented trigonal prism J50
BTPR-8	10 C2v	Biaugmented trigonal prism
JSD-8	11 D2d	Snub diphenoid J84
TT-8	12 Td	Triakis tetrahedron
ETBPY-8	13 D3h	Elongated trigonal bipyramid

Structure [ML8]	OP-8	HPY-8	HBPY-8	CU-8	SAPR-8	TDD-8	JGBF-8	JETBPY-8	JBTPR-8	BTPR-8	JSD-8	TT-8	ETBPY-8
ABOXIY,	33.065,	26.453,	13.031,	11.430,	5.166,	2.780,	8.764,	25.516,	4.149,	4.026,	2.649,	12.251,	21.925

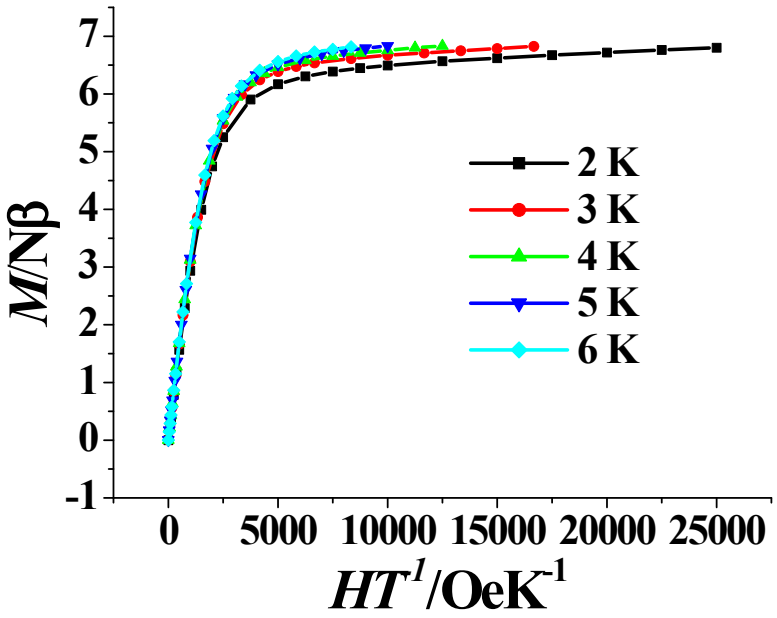

Fig. S4. *M* versus *H*/*T* plots at 2-6 K of **1**.

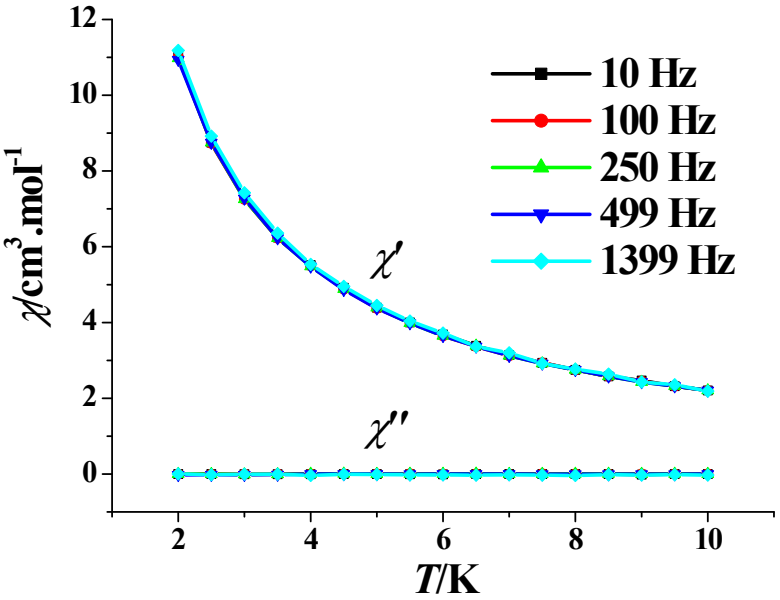

Fig. S5. Temperature dependence of χ' and χ'' for **1** under zero dc field.

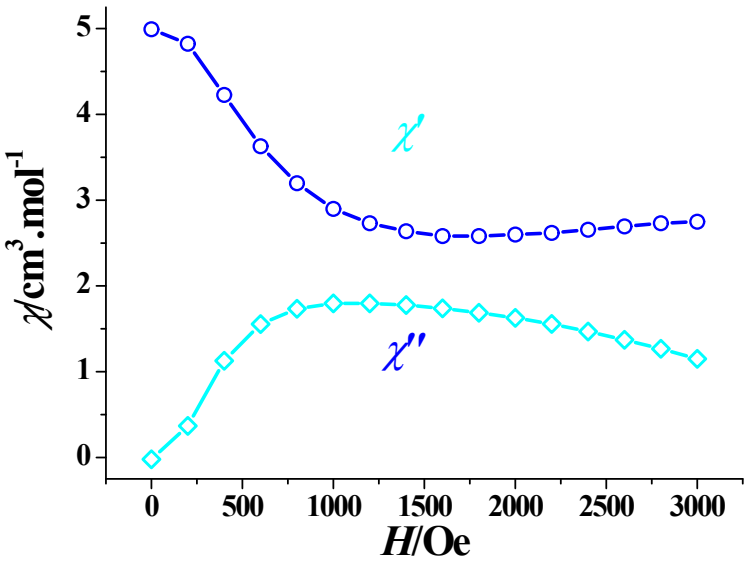

Fig. S6. AC susceptibilities measured at 2.5 Oe ac magnetic field with variable dc fields at 997 Hz and 4 K for **1**.

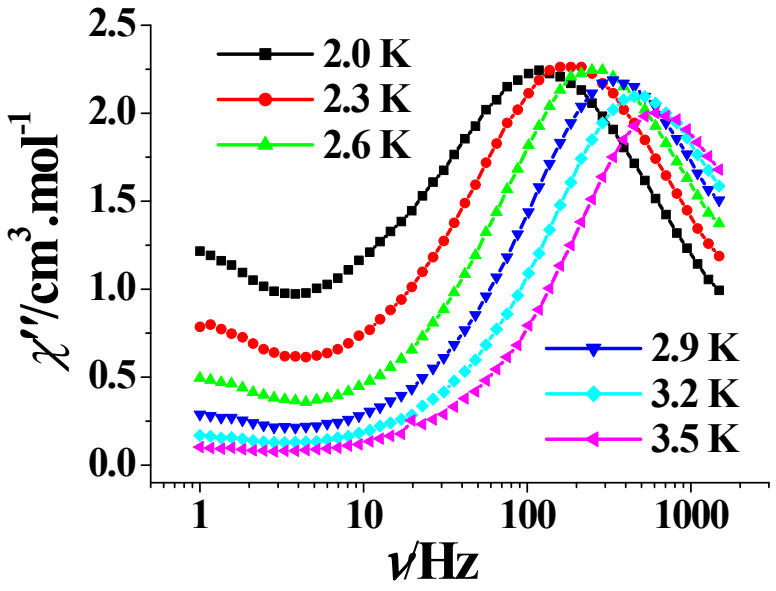

Fig. S7. Frequency dependence of χ'' for **1** under 1k Oe dc field.

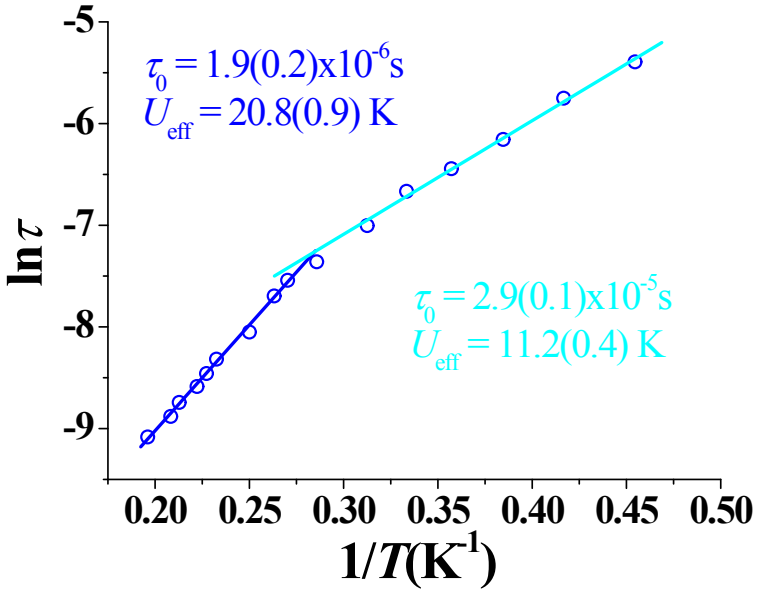

Fig. S8. Plot of ln(τ) versus 1/T for **1,** the solid line represents the best fitting with the Arrhenius law.

Table S2. Linear combination of two modified Debye model fitting parameters from 2.0 K to 3.5 K of **1** under 1k Oe dc field.

T(K)	χ_2(cm^3.mol^{-1})	χ_1(cm^3.mol^{-1})	χ_0(cm^3.mol^{-1})	τ_1(s)	α_1	τ_2(s)	α_2
2.0	10.32048	3.15118	0.13503	0.30717	0.1847	0.00124	0.30177
2.3	8.42254	1.69027	0.31664	0.18177	0.00165	0.00082	0.2514
2.6	7.52766	1.33708	0.52916	0.17744	7.3285E-6	0.00057	0.20472
2.9	6.76246	1.0898	0.68687	0.16241	0.00006	0.00042	0.16426
3.2	6.1953	1.03945	0.79636	0.1753	3.2011E-6	0.00032	0.12956
3.5	5.72272	0.99197	0.82737	0.20102	0.00001	0.00024	0.10561

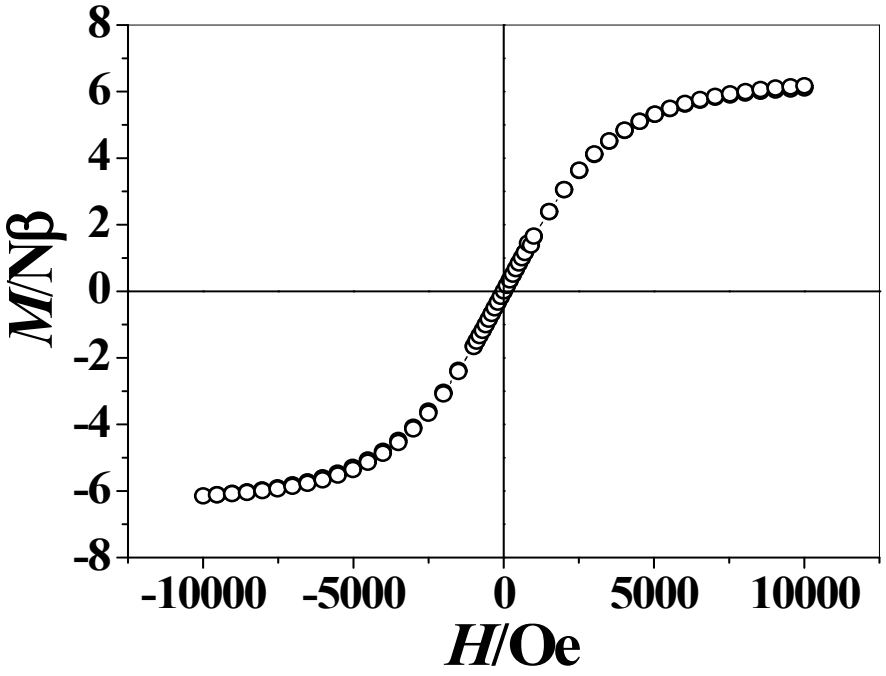

Fig. S9. Hysteresis loop for **1** at 1.9K.

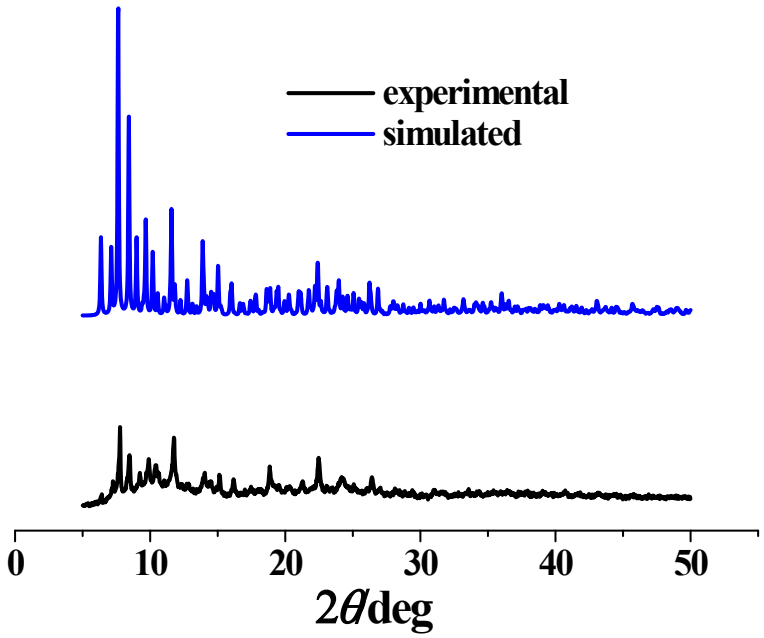

Fig. S10. The simulative and experimental powder X-ray diffraction patterns for **2**.

Table S3. Continuous Shape Measures calculation for Dy1 atom in **2**.

Dy1 structure

OP-8	1 D8h	Octagon
HPY-8	2 C7v	Heptagonal pyramid
HBPY-8	3 D6h	Hexagonal bipyramid
CU-8	4 Oh	Cube
SAPR-8	5 D4d	Square antiprism
TDD-8	6 D2d	Triangular dodecahedron
JGBF-8	7 D2d	Johnson gyrobifastigium J26
JETBPY-8	8 D3h	Johnson elongated triangular bipyramid J14
JBTPR-8	9 C2v	Biaugmented trigonal prism J50
BTPR-8	10 C2v	Biaugmented trigonal prism
JSD-8	11 D2d	Snub diphenoid J84
TT-8	12 Td	Triakis tetrahedron
ETBPY-8	13 D3h	Elongated trigonal bipyramid

Structure [ML8]	OP-8	HPY-8	HBPY-8	CU-8	SAPR-8	TDD-8	JGBF-8	JETBPY-8	JBTPR-8	BTPR-8	JSD-8	TT-8	ETBPY-8
ABOXIY,	30.938,	23.798,	15.886,	10.365,	1.945,	0.678,	13.642,	29.468,	2.161,	1.365,	3.022,	11.166,	25.720

Table S4. Continuous Shape Measures calculation for Dy2 atom in **2**.

Dy2 structures

OP-8	1 D8h	Octagon
HPY-8	2 C7v	Heptagonal pyramid
HBPY-8	3 D6h	Hexagonal bipyramid
CU-8	4 Oh	Cube
SAPR-8	5 D4d	Square antiprism
TDD-8	6 D2d	Triangular dodecahedron
JGBF-8	7 D2d	Johnson gyrobifastigium J26
JETBPY-8	8 D3h	Johnson elongated triangular bipyramid J14
JBTPR-8	9 C2v	Biaugmented trigonal prism J50
BTPR-8	10 C2v	Biaugmented trigonal prism
JSD-8	11 D2d	Snub diphenoid J84
TT-8	12 Td	Triakis tetrahedron
ETBPY-8	13 D3h	Elongated trigonal bipyramid

Structure [ML8] OP-8 HPY-8 HBPY-8 CU-8 SAPR-8 TDD-8 JGBF-8 JETBPY-8 JBTPR-8 BTPR-8 JSD-8 TT-8 ETBPY-8

ABOXIY, 32.373, 24.804, 12.411, 11.078, 5.167, 2.875, 8.466, 24.080, 3.875, 3.729, 2.717, 11.826, 20.690

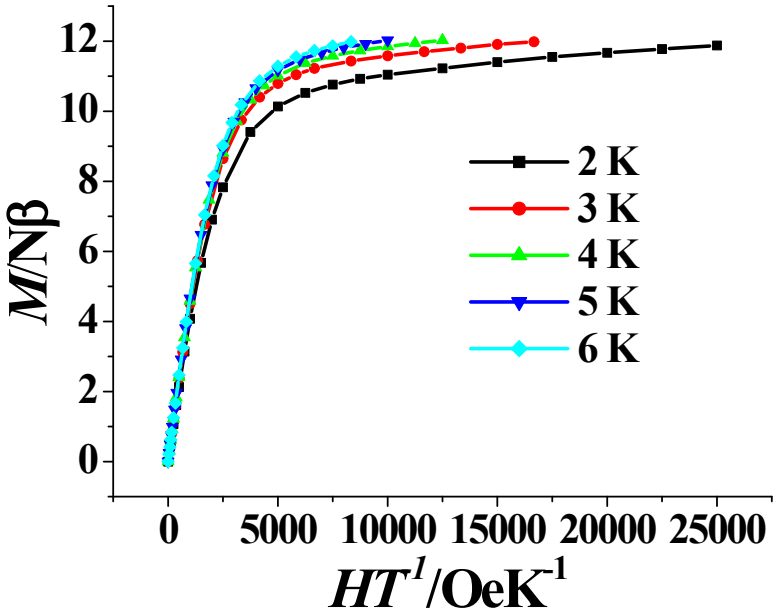

Fig. S11. *M* versus *H*/*T* plots at 2-6 K of **2**.

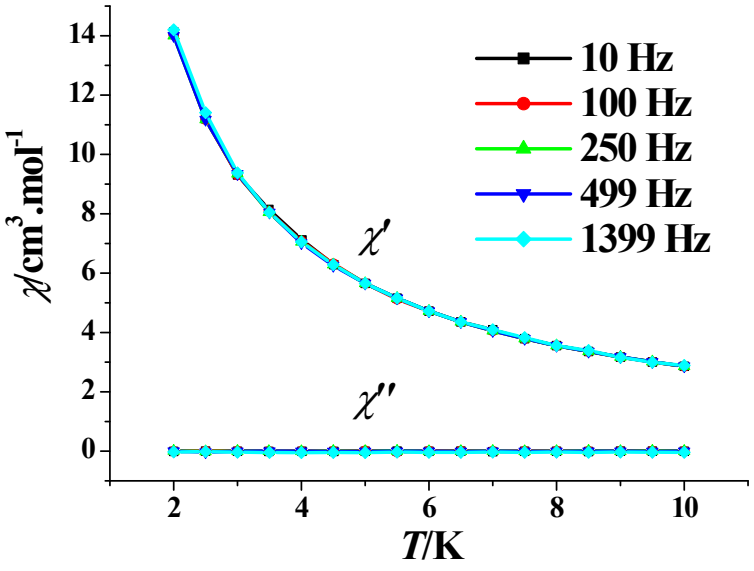

Fig. S12. Temperature dependence of χ' and χ'' for **2** under zero dc field.

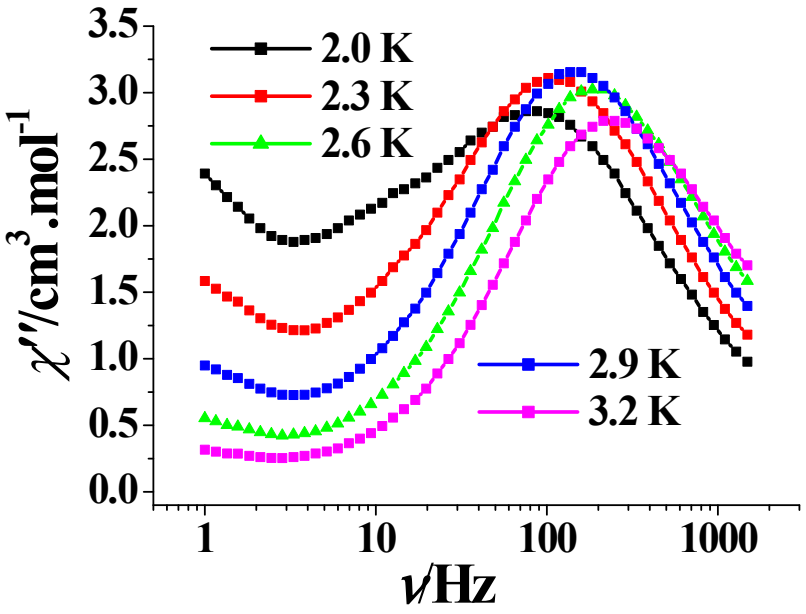

Fig. S13. Frequency dependence of χ'' for **2** under 1k Oe dc field.

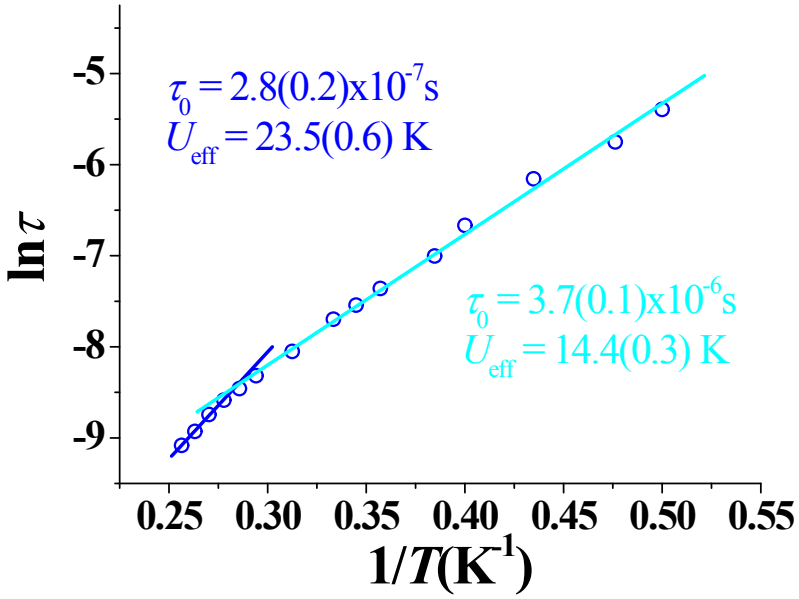

Fig. S14. Plot of ln(τ) versus 1/T for **2,** the solid line represents the best fitting with the Arrhenius law.

Table S5. Linear combination of two modified Debye model fitting parameters from 2.0 K to 3.2 K of **2** under 1k Oe dc field.

T(K)	χ_2(cm^3.mol^{-1})	χ_1(cm^3.mol^{-1})	χ_0(cm^3.mol^{-1})	τ_1(s)	α_1	τ_2(s)	α_2
2.0	15.91434	6.45311	0.17806	0.34886	0.23473	0.00198	0.33104
2.3	13.33996	9.91133	0.46103	0.00143	0.26928	0.28356	0.10259
2.6	11.84799	9.79794	0.72298	0.00104	0.23039	0.32001	0.01467
2.9	9.42824	10.76502	0.97566	0.00077	0.20948	0.43492	0.00002
3.2	12.55688	4.91849	1.25066	2.44045	0.00012	0.0006	0.19301

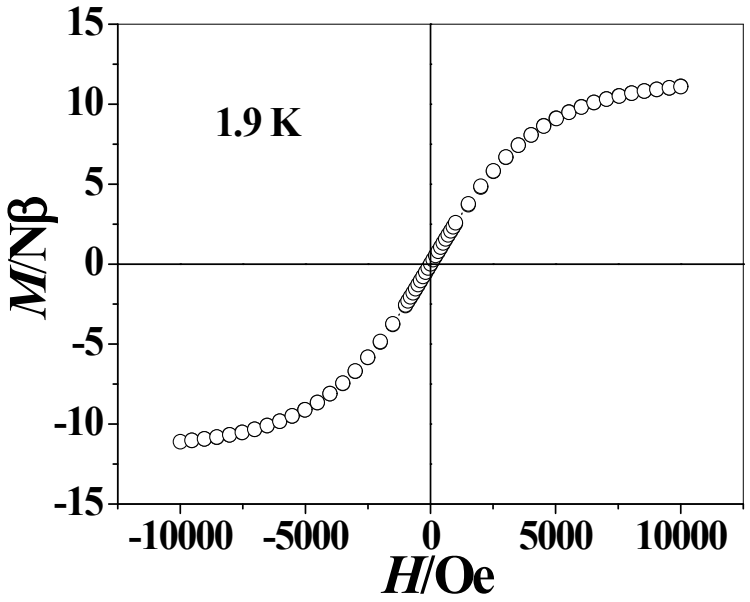

Fig. S15. Hysteresis loop for **2** at 1.9K.